Journal Name

ARTICLE

A Bimodal Fluorescent and Photocytotoxic Naphthalene Diimide for Theranostic Applications

Received 00th January 20xx,
Accepted 00th January 20xx

DOI: 10.1039/x0xx00000x

www.rsc.org/

Erica Salvati, [c] Filippo Doria,[a] Francesco Manoli,[b] Carmen D'Angelo, [c] Annamaria Biroccio, [c] Mauro Freccero*[a] and Ilse Manet.*[b]

We report on the potential of a water-soluble tetracationic quaternary ammonium naphthalene diimide (NDI) as multifunctional agent of interest for theranostic applications. DNA binding ability of this NDI has been investigated. NDI exhibits high binding constants for G-quadruplex DNA but it is not selective for this type of DNA. Taking advantage of its intrinsic fluorescence and singlet oxygen sensitizing ability, cellular uptake, cytotoxicity and photocytotoxicity have been investigated. The intense emission in the Red/NIR, allows to monitor the cell permeability of this charged tetracationic NDI, accumulating into the cell nuclei. No dark cytotoxicity has been observed on selected tumor cell lines. Irradiation of the NDI loaded cells with red light reduces cell viability up to 40% and causes a significant increase of the percentage of cells expressing γH2AX foci indicating DNA damage. The presence of distinct DNA damage foci inside the nucleus suggests that the NDI molecule might induce DNA damage in specific sites. To the best of our knowledge this is the first NDI exhibiting PDT activity at μM concentration combined with low dark cytotoxicity.

Introduction

Core-substituted naphthalene diimides (NDI) have been widely explored as very appealing scaffolds because of their chemical accessibility and large planar aromatic surface paving the way for the design of multifunctional molecular systems. In the frame of biomedical applications, they have been studied both as fluorescent probes[1-3] as well as ligands targeting oligonucleotides.[4-9] The optoelectronic properties of NDI derivatives can be effectively tuned by introduction of one or more substituents on the aromatic core.[3, 10] Electron-rich substituents linked to the aromatic core give origin to an absorption band in the visible in addition to the high energy absorption band peaking at *ca.* 370 nm, typical of the NDI core, and an emission spectrum in the visible extending into the near-IR (NIR) region. Importantly for biomedical applications, water solubility has been achieved through the introduction of charged or ionizable substituents linked both to the aromatic core and to the diimide bridges. In this frame, we have prepared a library of neutral and cationic compounds starting from the NDI core introducing three or four amine substituents on the naphthalene diimide unit to engineer water soluble NDIs and in a recent article we preliminary reported their synthesis and photophysical characterization.[11] Among these, the selected tetracationic compounds **1** and **2** and the structurally related amines **3** and **4** (Scheme 1) exhibit promising properties as multifunctional molecular systems for theranostics.

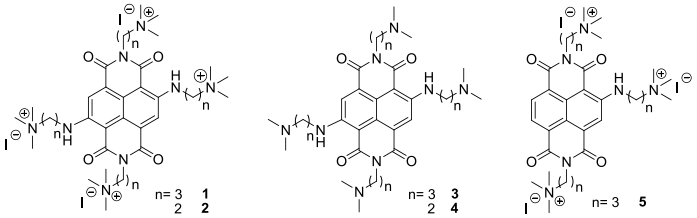

Scheme 1. Structure of the investigated tetracationic NDI **1** and **2** and related analogues (**3**-**5**).

The NDIs **1**-**4** are water-soluble and exhibit an absorption spectrum in water that extends up to 680 nm with a maximum at 613 nm. They are all fluorescent emitting up to 800 nm with a fluorescence quantum yield between 0.17 and 0.27 which makes them very appealing for optical imaging techniques.[11] Among them, only **1** is able to sensitize singlet oxygen formation with a quantum yield (Φ_Δ) of 0.30,[11] a value interesting for application in photodynamic therapy (PDT).[12] Therefore, the NDI compound **1** exhibits potential bimodal activity as fluorescent probe and reactive oxygen species (ROS) photosensitizer upon excitation with red light falling within the so-called PDT therapeutic window. This bimodal activity is lacking in the amine analogues **3** and **4**.

[a] *Dipartimento di Chimica, Università di Pavia. V.le Taramelli 10, 27100 Pavia, Italy.*
[b] *Istituto per la Sintesi Organica e la Fotoreattività, Consiglio Nazionale delle Ricerche, via Gobetti 101, 40129 Bologna, Italy*
[c] *Oncogenomic and Epigenetic Unit, Regina Elena National Cancer Institute, Via Elio Chianesi, 53 Rome, Italy*

† Footnotes relating to the title and/or authors should appear here.
Electronic Supplementary Information (ESI) available: [details of any supplementary information available should be included here]. See DOI: 10.1039/x0xx00000x

Table 1. Oligonucleotides used for the binding study in buffer solutions rich in K^+

Acronym	Origin	Sequence	Structure Type
Tel22, K^+	Human Telomeric DNA	5'-[$AG_3(T_2AG_3)_3$]-3'	Hybrid [3+1] G4[13]
c-myc2345	*c-myc promoter*	5'-[$GAG_3TG_4AG_3TG_4AAG$]-3'	Parallel G4[14, 15]
AS1411	Nucleolin binding aptamer	5'-[$GGT]_4TG[TGG]_4$-3	Parallel G4[16]
ds26mer	self-complementary ds DNA	5'-[$CA_2TCG_2ATCGA(AT)TCGATC_2GAT_2G$]-3'	duplex DNA

As mentioned above NDIs are known also as oligonucleotide ligands. Indeed, during the last decade it has been shown that tri- and tetra-substituted NDIs are potent and reversible ligands[7, 9, 17, 18] as well as selective alkylating agents targeting guanine-rich oligonucleotide sequences folded into G-quadruplex (G4) structures.[4, 19, 20] Guanine-rich sequences are present in biologically relevant proto-oncogenes and oncogene promoters[21] as well as human telomeres and participate in biological processes crucial for cell replication and survival.[22] They are known to adopt a G4 structure in solution and there is growing evidence that they do the same also in cells.[23] Maintenance of the DNA telomeres, characterized by tandem arrays of the sequence 5'-TTAGGG-3', is upregulated in almost all types of tumor cells thus having apparently unlimited capacity to proliferate.[24] Consequently, guanine-rich sequences represent a very appealing target propelling the research for the development of new approaches in cancer therapy. It has been shown that several NDIs exhibit high affinity for G4 in solution and the substitution pattern of the NDI core as well as the chemical nature of the substituents play a crucial role in the G4 binding and its selectivity toward G4 rather than duplex DNA.[6, 7, 17] In particular, substituents ending with amine groups resulted in strongly binding G4 ligands.[2, 4, 19] Neidle et al. have shown that in a crystal structure $\pi-\pi$ stacking of the NDI naphthalene core with the G-tetrad occurs while the positively charged subsituents protrude into the G4 grooves and interact electrostatically with the phosphates of the DNA backbone.[17] Some of these NDIs resulted to be very cytotoxic on selected cancer cell lines.[7, 25]

On basis of above considerations we decided to carry out further investigations on compound **1**, both in solution and in vitro. In more detail, we evaluated compound **1** as G4 ligand and investigated its photocytotoxicity in selected cell lines. In this context, the tetracationic character of **1** may represent a drawback for cell internalization. In order to circumvent possible internalization problems we also explored the aptamer AS1411 adopting a G4 structure as "Trojan horse" for intracellular delivery of **1**. The aptamer AS1411 recognizes specifically nucleolin, a multifunctional nuclear ribonucleoprotein present on the cell surface and overexpressed in some cancer cells.[26] Upon binding to the nucleolin the aptamer is shuttled inside the cell. Actually it is in clinical phase 2 for cancer therapy for the treatment of acute myeloid leukemia.[27] Several types of drug delivery systems have been modified with the aptamer AS1411 in order to improve their target specificity. [28] Just few examples are known for the delivery of drugs with only the aptamer as delivery tool.[29] In one case a cationic porphyrin TMPyP has been delivered by means of its non-covalent binding to AS1411 assuming a G4 structure.[30]

In this article, we report on the binding of **1** to G4 structures as well as duplex DNA in K^+ rich solutions. The cell permeability and compartmentalization of **1** in a panel of different human tumor cell lines has been assessed, taking advantage of the intrinsic fluorescence properties of **1**. Finally, we describe for the first time the ability of an NDI compound, in particular **1**, to act as photosensitizer for the light-induced generation of reactive oxygen species in selected cell lines and compare its behavior with a known PDT agent aminolevulinic acid, ALA.[31] For the first part of this study we have chosen three different G-rich sequences (Table 1): a telomeric sequence adopting a hybrid structure (Tel22),[13] the G-rich sequence of the c-Myc oncogene assuming a parallel structure (*c-myc*2345)[14, 15] and the aptamer AS1411 adopting an inter- and intramolecular parallel G4 structure.[16] We have investigated the affinity of compound **1** for DNA in duplex form using as model a self-complementary oligonucleotide of 26 bases, ds26mer, hybridizing in solution. Binding of **1** has been assessed by means of titrations monitoring absorption, fluorescence and circular dichroism features. The binding model and constants have both been obtained upon multiwavelength global analysis of the titration data.

Results and discussion

DNA Binding study of 1. The absorption spectrum of compound **1** in buffer solution in the presence of 100 mM K^+ is shown in Figure 1a. The absorption band with vibronic signature in the 300-400 nm range is typical of the aromatic NDI core.[32] The second absorption band peaking in the red at 613 nm is due to the introduction of two amine substituents on the NDI core and has origin in a charge transfer state transition. As said above this second band falls in the window of interest for biological applications such as cellular and tissue imaging as well as photodynamic therapy.[12] The fluorescence spectrum of compound **1** with maximum at 650 nm shown in Figure 1b extends up to 800 nm in the NIR. Compound **1** has a fluorescence quantum yield of 0.17 and a fluorescence lifetime of 4.8 ns in this K^+ rich buffer.[11]

To study the binding behavior towards different types of DNA in K^+-rich phosphate buffer compound **1** has been titrated with different amounts of DNA reaching an excess concentration of 3-4 times NDI concentration. Figures 1a-c show the experimental data obtained for titration of **1** with Tel22 (see Table 1 for sequence) monitored by means of absorption, fluorescence and circular dichroism. Titrating compound **1**

Journal Name

ARTICLE

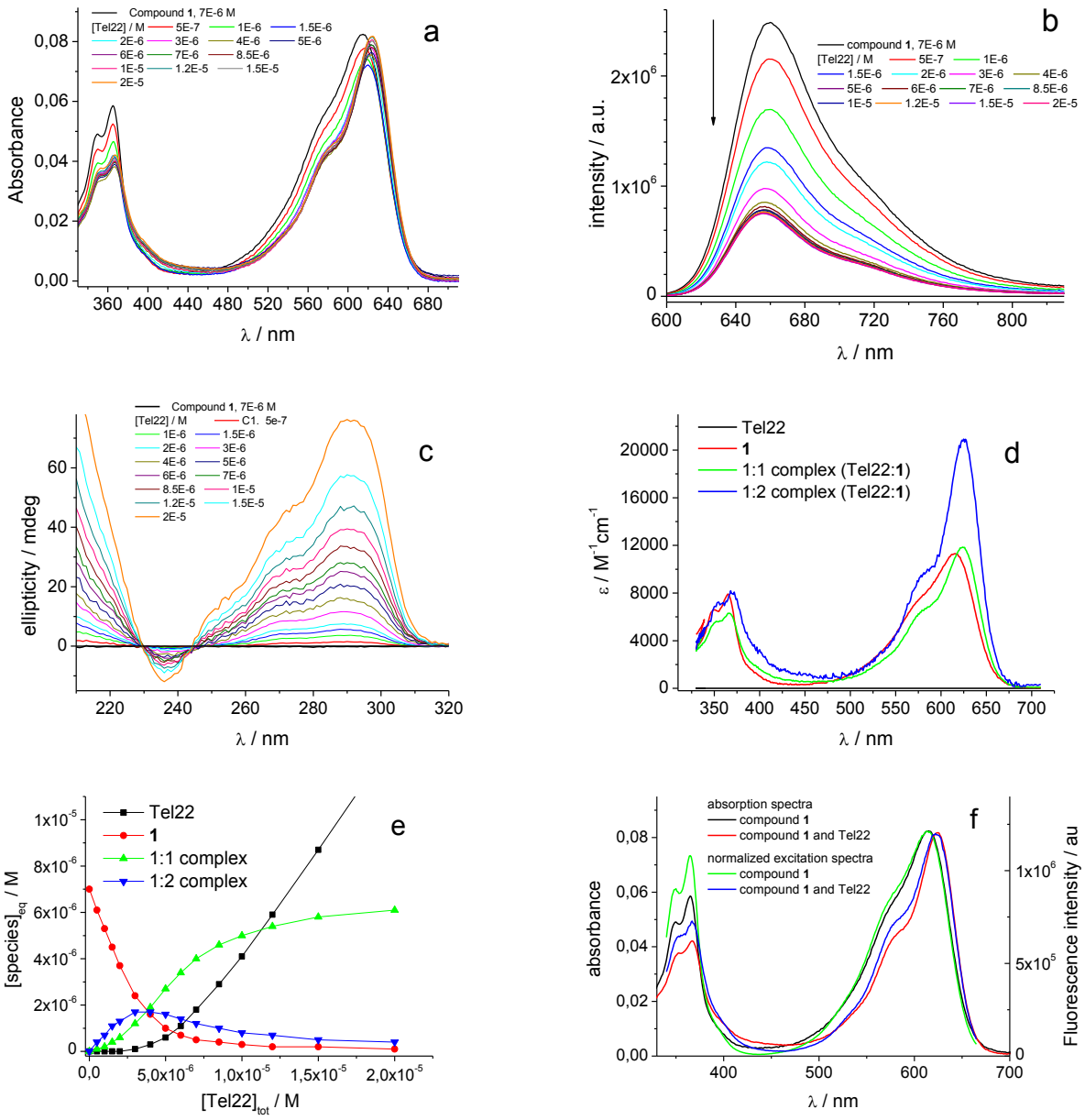

Figure 1. a. Absorption spectra of a 7.0×10^{-6} M solutions of **1** with increasing Tel22 concentration (range 0.5×10^{-6}-2.0×10^{-5} M) in phospate/KCl buffer, pH 7.0; **b.** Fluorescence spectra, idem; **c**. Circular dichroism spectra of a 7.0×10^{-6} M solutions of **1** with increasing Tel22 concentration (range 0.5×10^{-6}-2.0×10^{-5} M) in phospate/KCl buffer, pH 7.0; note: spectrum of **1** alone in Figure 1a-c is black; **d**. Calculated absorption spectra of the free species and the complexes obtained for the binding constants $\log(K_{11}/M^{-1}) = 6.61 \pm 0.05$, $\log(K_{12}/M^{-2}) = 12.37 \pm 0.20$; **e**. Species equilibrium concentration in the mixtures versus total Tel22 concentration calculated with the binding constants $\log(K_{11}/M^{-1}) = 6.61 \pm 0.05$, $\log(K_{12}/M^{-2}) = 12.37 \pm 0.20$; **f**. Normalized fluorescence excitation spectra of a 7.0×10^{-6} M solutions of **1**, free and with excess Tel22, compared with the absorption spectra;

with the other types of G4 DNA in Table 1 we have observed similar complexation behavior and in the following we will only evidence the differences. We refer to S.I. for the data of the other types of G4 DNA (S.I. Figures 2-3). Binding to G4 DNA is evidenced by the 10 nm shift of the red absorption maximum of **1** to 623 nm. Quenching of the fluorescence intensity of **1**

upon addition of increasing amounts of G4 DNA is also indicative of complexation and is likely due to electron transfer from the guanine residues to the NDI moiety. The CD spectra in the UV of **1** in the presence of Tel22 have the characteristics of complexes with G4 in hybrid form showing a positive peak at 292 nm and a shoulder at 270 nm. No induced CD signals have been observed in correspondence of the NDI absorption bands. The experimental data differ for solutions of **1** and Tel22 that have been heated for 20 minutes at 50°C before performing measurements. The latter results have been reported in S.I. Figure 1. The different behavior is inferred to the presence of complexes with other conformations in solution. Indeed, the CD spectra of the mixtures in the UV allow concluding safely that heating shifts the complexation equilibrium toward the formation of complexes with the Tel22 adopting a parallel G4 conformation especially in the presence of excess NDI. The mixtures that have not been heated undergo the same transition from hybrid G4 to parallel G4 complexes when kept in the dark for 24 or 48 hours. We will discuss this further in the paragraph dealing with melting.

Global analysis (GA) of the multiwavelength data set corresponding to the absorption spectra of the different mixtures of Tel22 in Figure 1a allowed to determine the best complexation model, the binding constants of the most stable complexes (Table 2) as well as the individual absorption spectra of the associated species (see Figure 1d). In the case of the other two sequences adopting a parallel G4 structure, *c-myc*2345 and AS1411, we have obtained the same binding model. The log values of their binding constants are also reported in Table 2. Complexation in the latter two cases did not cause any significant change in the UV CD spectra, suggesting that the parallel conformation is maintained in the complexes, neither induced a CD signal in correspondence of the NDI absorption bands. The complexation model leading to convergence in multiwavelength GA foresees the presence of two complexed species with 1:1 and 1:2 (DNA:**1**) stoichiometry.

Table 2. Stoichiometry and binding constants obtained from multiwavelength global analysis of the titration absorption spectra measured in K^+ rich solutions[a]

DNA	Stoichiometry DNA:Ligand	pK_{11} (M^{-1}) / pK_{12} (M^{-2})[a]
hTel22	1:1	6.61± 0.05
	1:2	12.37± 0.20
***c-myc*2345**	1:1	5.79± 0.44
	1:2	12.16± 0.94
AS1411	1:1	5.94± 0.08
	1:2	12.91± 0.14
ds26mer	1:2	12.48± 0.11

[a] K_{1i} binding constant obtained from multiwavelength global analysis of the absorption titration data with the commercially available program Reactlab Equilibria

As to the absorption band in the visible no relevant hypochromic effects can be appreciated for the complexes with G4 DNA and supports that intercalation, evidenced by hypochromicity reaching 60% absorbance reduction, of NDI between tetrads is not occurring.[5, 33] This effect is less pronounced for *c-myc*2345 and AS1411. The same binding model has emerged from GA of the fluorescence data but it was necessary to fix the binding constant of the 1:1 complex to the value obtained from the absorption data. All NDI species, free and complexed, have been indicated as fluorescent in the global analysis. The excitation spectra obtained for solutions with an excess of DNA show a maximum at 622 nm, which is shifted to the red with respect to the maximum observed in the excitation spectrum of the free NDI species (see Figure 1f) thus confirming that complexed species are emissive. Also the fluorescence lifetime of **1** changes upon interaction with different G4 topologies. Fluorescence decays for excitation at 373 nm, have been recorded for **1** alone and in the presence of varying concentrations of DNA. GA of the sets of fluorescence decays required a 4-exponential fitting function to converge. One lifetime, that of the free compound **1** in K^+ rich phosphate buffer, 4.84 ns, has been fixed. In the case of Tel22 GA has yielded three lifetimes of 0.31, 2.08 and 6.89 ns apart from the fixed free species lifetime. The average fluorescence lifetime of the mixtures gradually shortens with increasing DNA concentration to 1.98 ns. GA has afforded all the pre-exponential factors of the four lifetimes along the series of decays. The pre-exponential factors are linearly related to the concentration of the species emitting. Figure 1e shows the species concentrations at equilibrium obtained with the binding constants $\log(K_{11}/M^{-1})$ = 6.61 ± 0.05, $\log(K_{12}/M^{-2})$ = 12.37 ± 0.20. Along the series of decays the pre-exponential value of the lifetime of the free compound **1** decreased with increasing DNA concentration as this species disappears. The pre-exponential values of the lifetime of 6.89 ns continuously increased with increasing DNA concentration. Most likely it belongs to the population of the 1:1 complexes. Finally, the pre-exponential values of the shorter lifetimes of 0.31 and 2.08 ns have a trend in line with the variation of the 1:2 complex concentration, it increases initially and then reaches a plateau.[34] Considering that we have a mixture of at least two complex conformations for Tel22, parallel and hybrid, it is not straightforward to understand whether the two lifetimes belong to different complexation sites or different conformations. Also in the case of the binding of **1** to *c-myc2345* we have found 4 lifetimes, 0.42, 1.33, 4.84 (fixed, as it is due to free **1**) and 6.10 ns, even though the G4 conformation is only the parallel one. Our evidence, together with the recent finding that G4 ligands bind to a given G4 structure at distinct G-tetrads with differential binding affinities[35] suggest that fluorescence lifetime measurements might be able to recognize ligand interaction with either the top or the bottom G-tetrad.

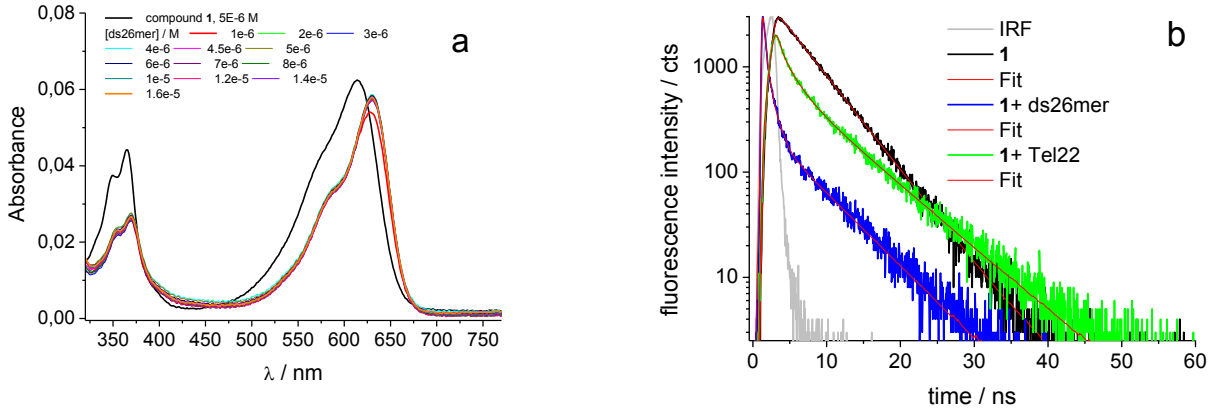

Figure 2. a. Absorption spectra of a 5.0×10^{-6} M solutions of **1** with increasing ds26mer concentration (range 1×10^{-6}-1.6×10^{-5} M) in phospate/KCl buffer, pH 7.0; **b.** Fluorescence decay of **1** alone (black) and in the presence of an excess of Tel22 (green) and ds26mer (blue).

Indeed, the local NDI environment, depending on the G-tetrad as well as the loops nearby, in different binding sites is likely determining for the fluorescence lifetime. In the 1:2 complexes we also need to keep in mind that self-quenching between spatially close NDI molecules can occur and account for shorter lifetimes.

Finally, we evaluated binding to a duplex strand. The self-complementary sequence ds26mer can adopt in solution a helix making two complete turns. In addition, in this case we have observed a red shift of the absorption maxima (Figure 2a) and strong quenching of the fluorescence. (See S.I. Figure 4) There is a small hypochromic effect in the high-energy band of the absorption spectra of the complexes while the effect is much more pronounced for the UV band. Further, the CD spectra in the UV are not changing shape during titration. So, we can likely exclude intercalation of the NDI in the duplex since this generally results in strong hypochromic effects and changes in the CD spectra due to double helix conformational changes upon intercalation.[33] Groove binding thus seems reasonable for ds26mer. Noticeably, only in this case we have observed an induced circular dichroism (ICD) spectrum in the visible in correspondence with the NDI absorption bands. In the case of duplex DNA of the self-complementary ds26, the analysis converged only with a complexation model of one fluorescent complex with 1:2 stoichiometry. Considering the Tel22 and ds26mer binding constants, **1** is not selective for Tel22 (Table 2). GA of the fluorescence decays in the presence of different amounts of ds26mer has yielded three fluorescence lifetimes for the 1:2 complexes, 0.22, 0.84 and 6.10 ns together with the 4.84 ns lifetime of the free species. The pre-exponentials of the two short lifetimes were significantly larger than that of the long lifetime and resulted in an average lifetime significantly shorter for the mixtures of **1** with ds26mer (Figure 2b). This feature has been exploited in fluorescence lifetime imaging, see below.

For the sake of comparison, we also examined the behaviour of tri-substituted compound **5** (Scheme 1) with Tel22. The log values of the binding constants are $\log(K_{11}/M^{-1}) = 6.77 \pm 0.02$, $\log(K_{21}/M^{-2}) = 13.30 \pm 0.01$. Noticeably, the fluorescence of **5** is completely quenched in the complex (S.I. Figure 5). This supports the hypothesis that electron transfer from guanine residues to NDI is responsible for quenching since the tri-substituted compound **5** is a much better photo-oxidant than the tetra-substituted compound **1**. The absence of fluorescence in the complex makes this molecule less appealing from the point of view of biomedical applications based on fluorescence imaging.

DNA Melting studies in the presence of 1. We checked the stability of the complexes with a melting study. The *c-myc2345* complexes were not tested due to the high melting temperature above 80°C of this sequence.[15] Free Tel22 has a melting temperature around (65°C) obtained from a UV absorption experiment in agreement with literature data (~67°C) for similar buffers.[35] Note that in the mixture of **1** and Tel22 we have ca. 55 % of DNA present as 2:1 complex, 40 % as 1:1 complex and a very little fraction of free DNA. The initial circular dichroism (CD) spectrum of the mixture seems to be dominated by the features of the hybrid complex conformations with a maximum at 292 nm, while the shoulder around 270 nm is indicative of the presence of small amounts of other conformations likely the parallel one (see Figure 3a, black spectrum).

The melting curves obtained measuring ellipticity at diagnostic wavelengths (268 and 290 nm, Figure 3b) have evidenced that the complexes in the mixture have two different melting points. Ellipticity at 268 nm of the mixture reaches a maximum value at 66°C, and then decreases going to 90°C without anyway unfolding completely, while ellipticity at 268 nm and 290 nm of the free DNA decreases almost to zero for completely unfolded Tel22.

Journal Name

ARTICLE

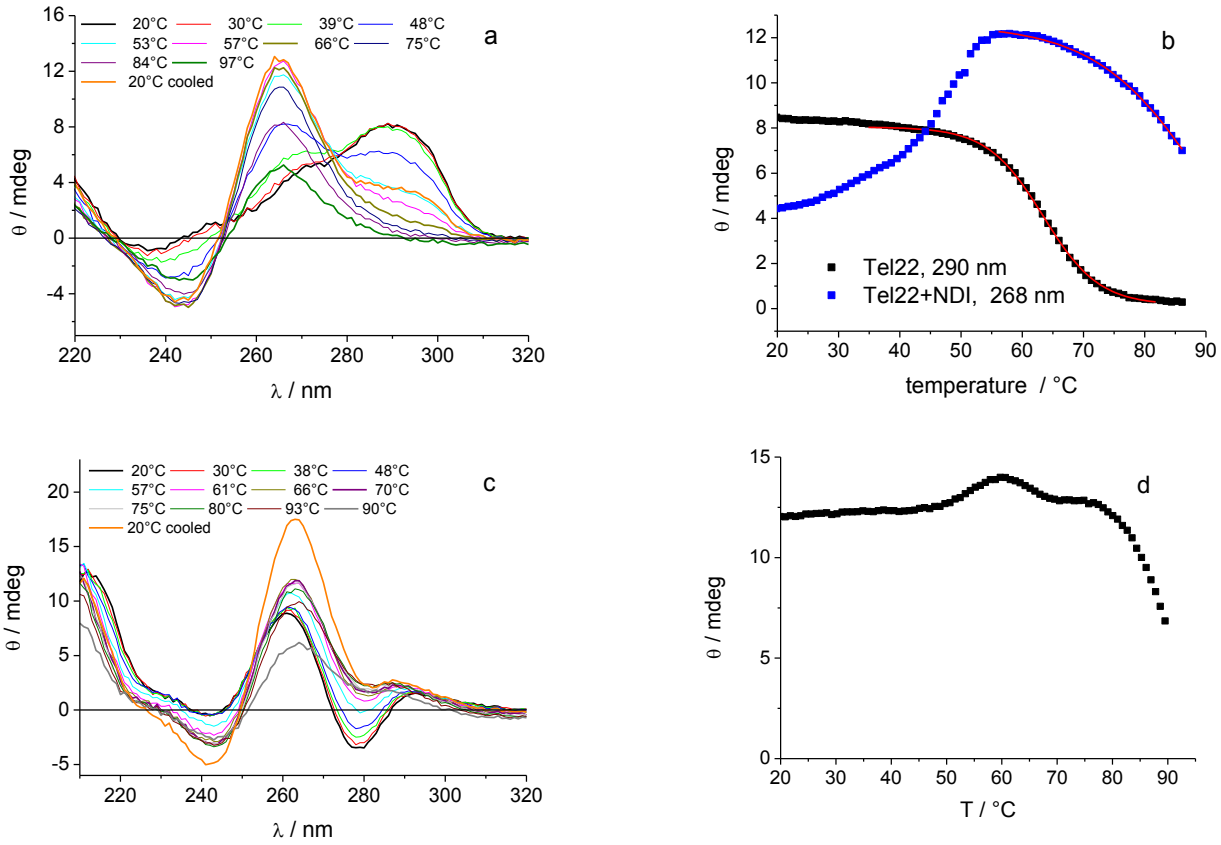

Figure 3. a. CD spectra of a mixture of Tel22 (2.0×10^{-6} M) and **1** (4.0×10^{-6} M) in 10 mM K^+ PB of pH 7.4 with 100 mM KCl at different temperatures including the spectrum at 20°C (orange) after the melting experiment. **b**. Ellipticity changes θ(T) of 2.0×10^{-6} M Tel22 solution (black) and of a mixture (blue) of Tel22 (2.0×10^{-6} M) and **1** (4.0×10^{-6} M) in 10 mM K^+ PB of pH 7.4 (a) at 290 nm (■) and 268 nm (■) with 100 mM KCl; error was ± 0.5 mdeg. **c**. CD spectra of a mixture of AS1411 (2.0×10^{-6} M) and **1** (4.0×10^{-6} M) in 10 mM K^+ PB of pH 7.4 with 100 mM KCl at different temperatures including the spectrum at 20°C (orange) after the melting experiment. **d**. Ellipticity changes θ(T) of a mixture of AS1411 (2.0×10^{-6} M) and **1** (4.0×10^{-6} M) in 10 mM K^+ PB of pH 7.4 with 100 mM KCl at 261 nm (■); error was ± 0.5 mdeg.

After cooling, the CD spectrum of the mixture is dominated by the typical features of the parallel complex with a positive peak at 265 nm and a less intense negative peak at 245 nm (Figure 3a). The hybrid complex seems to unfold and transform into a parallel complex with a melting temperature well above that of the free DNA, so clearly stabilized. The temperature derivative of the ellipticity curve in figure 3b obtained for the mixture of Tel22 and **1** gives a melting point at 48°C below that of free DNA. Applying a Boltzmann sigmoidal fit to the same ellipticity curve restricted to the data above 52°C, an inflection point of 87°C is calculated, fixing the final ellipticity to 0.8 (similar to free DNA). Applying the same Boltzmann sigmoidal fit to the free DNA melting curve in Figure 3b, yielded 63°C comparable to the value obtained from the temperature derivative of the ellipticity curve. We can estimate a stabilization temperature of 25°C for the complex in parallel form of compound **1** with Tel22. A somewhat similar behavior has been observed for the AS1411 sequence (Figure 3c). There is a transition to a G4 complex with different conformation and only above 75°C unfolding became visible (Figure 3d). As free AS1411 has a melting temperature of 73°C (S.I. Figure 6) we observe stabilization of the complex. Ds26mer has two melting temperatures of 65 and 75°C, obtained from the first temperature derivative; the presence of **1** does not change its melting temperature significantly so **1** is not stabilizing duplex DNA (SI Figure 6).

Cellular Permeability. The presence of four quaternary ammonium moieties (NMe^{3+}) could represent an important limiting factor in terms of cells permeability and biological

applications of this NDI. In fact, organic cation transporter systems are often required to implement human cellular permeability of small mono- and dicationic drugs.[36] Differently, tetracationic porphyrins with low degree of lipophilicity, which are related to our NDI in terms of charge and G4 binding properties, are cell permeable through endocytosis.[37] Neidle et al reported on the cellular uptake of NDIs with chargeable amine groups without specifying the uptake mechanism.[38] Taking advantage of the fluorescence properties of the molecule, we have performed the first biological test with the aim to analyze the cell permeability and compartmentalization of **1** in different human tumor cell lines. Qualitative analysis by fluorescence microscopy in living cells exposed to 5 μM solution of **1** for 12 hours clearly revealed that it is taken up into the cells and is transported into the nuclei in all the tumor cells analyzed (Hela, BJEHLT and U2OS, Figure 4A and S.I. Figure 7).

As internal control, nuclei of MCF7 breast cancer cells resistant to Adriamycin due to the overexpression of the ATP-dependent efflux pump P-glycoprotein (P-gp), resulted completely negative compared to the sensitive counterpart (MCF7 ADR, S.I. Figure 7) since the compound was actively shuttled out.[39] To quantify the amount of internalized compound **1** administered alone or complexed with the AS1411 aptamer, FACS analysis was performed after 6 or 16 hours of compound administration. Consistent with microscopy analysis, fluorescence intensities measurement revealed that **1** is cell permeable alone and in the presence of AS1411 and, as expected, the cellular uptake is increased by a longer drug exposure (Figure 4b). Quantitative analysis clearly showed that internalization of **1** did not improve when the drug was complexed with AS1411 at all the times analyzed (Figure 4b).

Cytotoxicity of 1. On the basis of the results obtained, the cytotoxicity of **1** and AS1411 (as single agents or as a complex) was determined in a MTT assay in a panel of human tumor cell lines by using different drug doses ranging from 0.5 to 100 μM. The results clearly showed that **1** alone does not reduce cell viability of tumor cells at all the times and drug doses analyzed (Figure 5 and S.I. Figure 8). Consistently with already reported data AS1411 alone decreases cell viability in a cell context dependent manner, reaching about the 40% of growth inhibition in BJEHLT and HeLa at the maximum dose used, whereas MCF7 and U2OS cells are completely unaffected by the same treatment

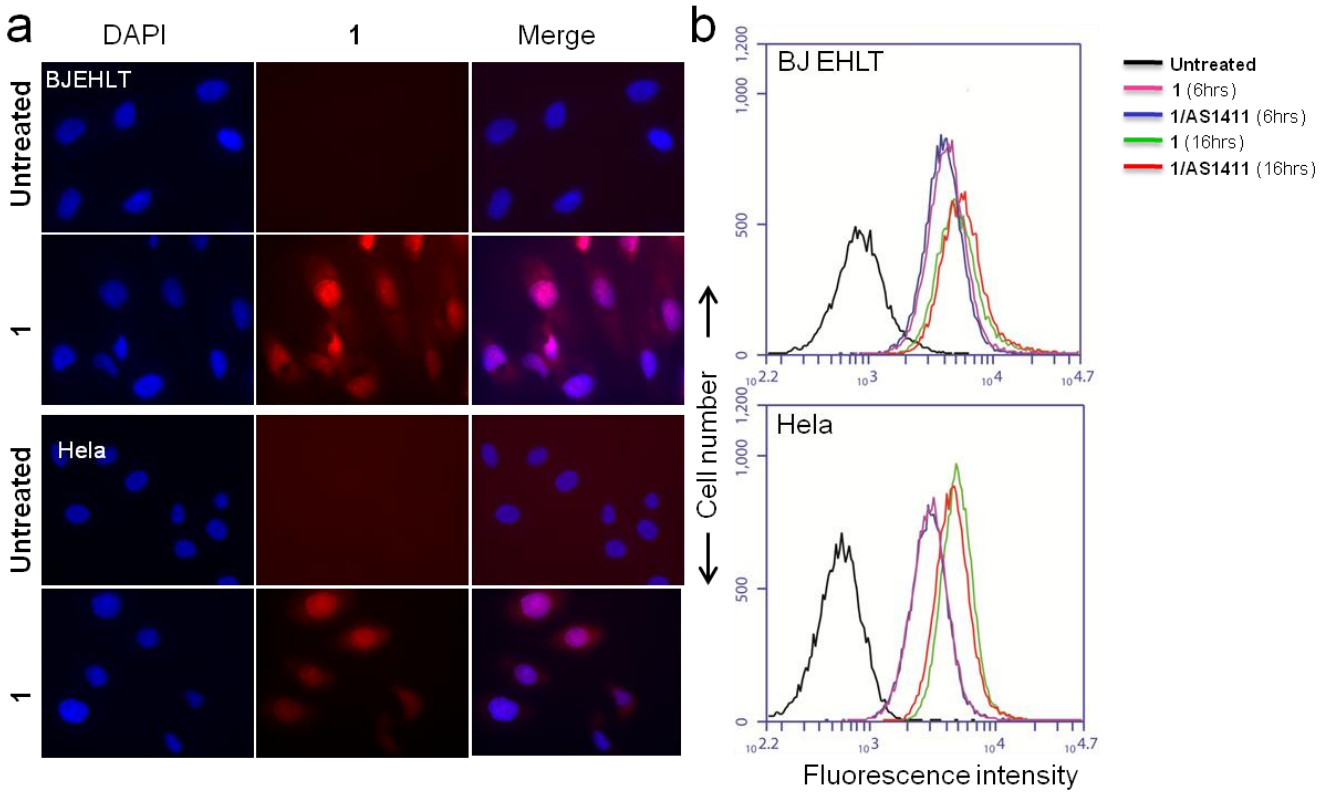

Figure 4. Qualitative and quantitative analysis of **1** uptake in presence or absence of AS1411. **a.** The indicated cell lines were exposed to 5 μM of **1** for 12 hours, then fixed, permeabilized and counterstained with DAPI. Fluorescence signals were analyzed with an inverted fluorescence microscope at 63X magnification. Pictures show representative images of DAPI staining and **1** fluorescence emission (Excitation filter 515-560 nm, Suppression filter LP 590 nm) in single and merged channels. **b.** Amount of internalized compound was measured by flow cytometry. Hela and BJEHLT (black histograms: untreated cells) were exposed to 5 μM **1** alone for 6 (pink histograms) or 16 hours (green histograms), or complexed with the AS1411 G4 for 6 (blue histograms) or 16 hours (red histograms). At the end of treatments cells were detached and the fluorescence intensity of internalized **1** was measured. One representative out of

three independent experiments is shown.

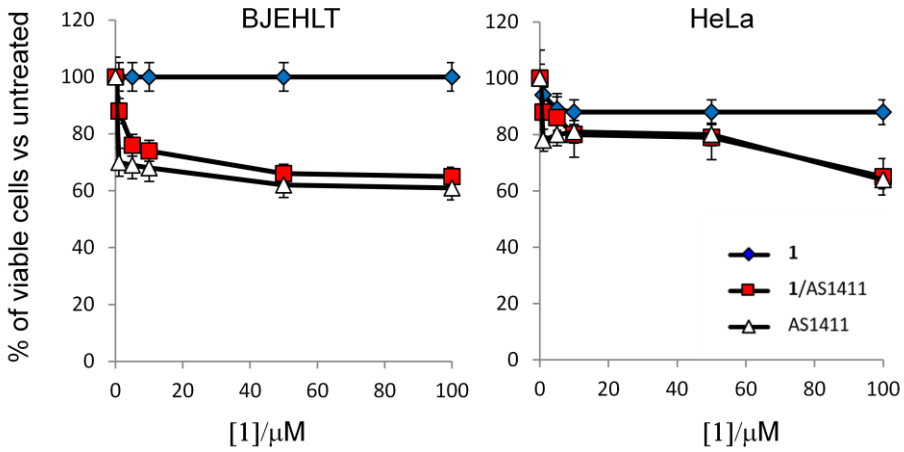

Figure 5. Cytotoxic effect of NDI in presence or absence of AS1411. BJEHLT and HeLa cells were chronically exposed to the indicated doses of **1** alone or complexed with AS1411 in a 1:2 molar ratio. Viability of cells was determined after 7 days treatment by MTT assay and expressed as percentage of cell viability compared to untreated samples. Histograms show the mean values of three independent experiments. Bars indicate means ±SD

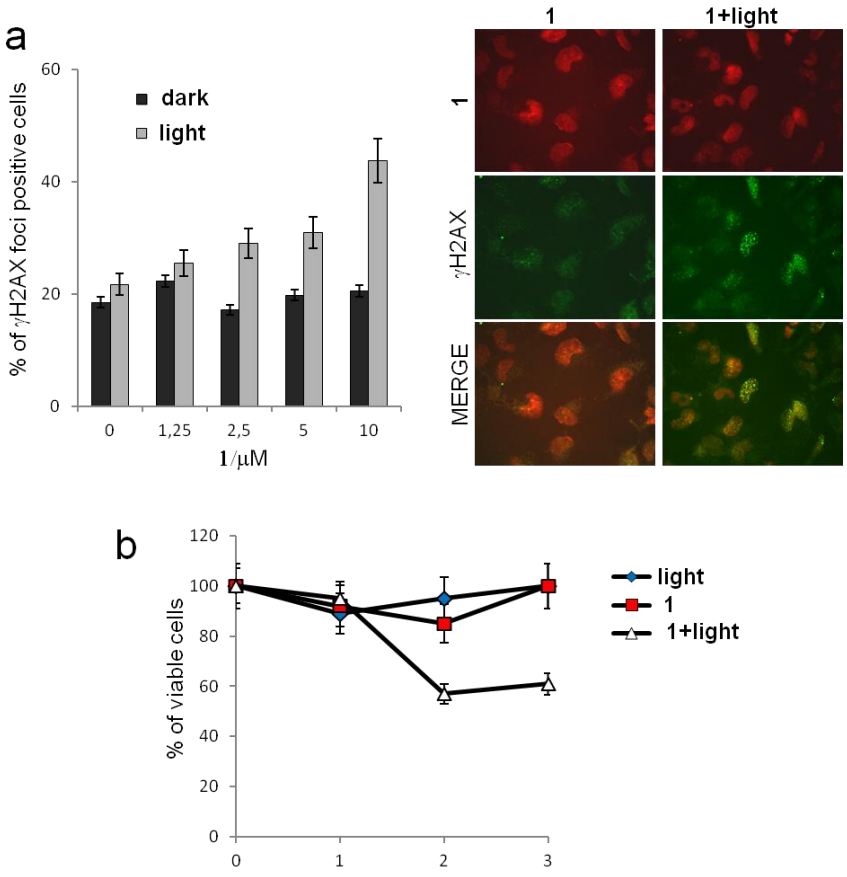

Figure 6. Light induced NDI cytotoxicity. BJEHLT fibroblasts were treated with 10 μM **1** for 12 hours and then exposed or not to PDT as described in the Experimental Section. **a.** For immunofluorescence detection of DNA damage foci, cells were fixed after 24 hours from PDT and stained with an anti-γH2AX antibody and counterstained with DAPI. Histograms report the percentage of γH2AX foci positive cells on total nuclei. Representative images show the presence of **1** within the nuclei of irradiated and non irradiated cells, and its co-localization with γH2AX foci upon irradiation (63X magnification). **b.** Cells treated as described above were detached and counted at the indicated time points after PDT to determine the number of viable cells. Curves report the percentage of viable cells in each condition, compared to not irradiated cells. Histograms show the mean values of three independent experiments. Bars indicate means ±SD.

conditions (S.I. Figure 8).[27] Significantly, this effect is comparable to that achieved by treating cells with the **1**/AS1411 complex, suggesting that the absence of cytotoxicity of **1** could be not merely due to a lack of binding to the cellular G4 DNA.

Photocytotoxicity of 1. The absence of general cytotoxicity of **1**, together with its ability to produce singlet oxygen species upon irradiation, makes this molecule potentially interesting for application in PDT. To this aim BJEHLT (a fibroblast derived cell line showing high sensitivity to the porphyrinogen 5-ALA - 5-aminolaevulinic acid- combined with photodynamic therapy, SI Figure 9) were treated with 10 μM of **1** for 12 hours to allow internalization, then the cells were exposed to irradiation with red light (λ_{max} = 630 nm) and DNA damage induction and viability were evaluated. The results demonstrated that irradiation *per se* does not activate a DNA damage response and, consistent with this result, does not influence the cellular viability (Figure 6b). Interestingly, a significant increase of the percentage of cells expressing γH2AX foci (a marker of DNA damage induction) accompanied by a decrease of cell viability of about 40% is observed in irradiated compared to non-irradiated samples in the presence of **1**. The presence of distinct DNA damage foci inside the nucleus, (Figure 6a, 2X enlargements) suggests that **1** could induce DNA damage in specific sites, not necessarily G4 sites. Confocal fluorescence lifetime imaging of fixed BJEHLT fibroblasts treated with **1** exciting at 640 nm, where **1** absorbs almost selectively, has given some further information (Figure 7). Fitting the fluorescence decay calculated for a region of interest corresponding to the nuclear area, we find two lifetimes, 1 ns and 4.7 ns. Interestingly, the 4.7 ns lifetimes coincides with the lifetime measured for compound **1** free in solution, while the 1 ns lifetime is very close to one of the lifetimes measured in the presence of the duplex ds26mer. Therefore, in the nucleus **1** is present both as free molecule as well as complexed to duplex DNA and this confirms our hypothesis that **1** binds Tel22 well in solution, but it is not specific for G4 DNA. This is also in agreement with the absence of dark cytotoxicity at the doses used for the days of exposure applied.

Conclusions

We have performed an accurate analysis of the potential of a tetracationic quaternary ammonium NDI to act as plurimodal agent for biomedical applications. First the G-quadruplex binding ability of this water soluble NDI has been investigated. Good binding constants have been obtained for G4 DNA but, unfortunately, the compound is not a selective ligand for G4 DNA. Starting from the ability of this NDI to act in solution as fluorescent dye and singlet oxygen sensitizer we have investigated cellular uptake, cytotoxicity as well as photocytotoxicity. The NDI intense emission in the Red/NIR allowed us to monitor for the first time the cell permeability of a permanently charged tetracationic NDI, which showed accumulation into the cell nuclei. Cell permeability did not improve using the non-covalent complex of **1** and the known aptamer AS1411 as delivery system. Irradiation of the NDI loaded cells with red light reduced cell viability up to 40% and caused a significant increase of the percentage of cells expressing γH2AX foci indicating DNA damage. The presence of distinct DNA damage foci inside the nucleus suggests that the NDI molecule might induce DNA damage in specific sites. The limited selectivity of **1** for G4 DNA *vs* ds DNA and the confocal fluorescence lifetime imaging data suggest however caution in the assignment of the damage to G-quadruplex sites. Overall, to the best of our knowledge this is the first NDI exhibiting PDT activity at μM concentration combined with low dark cytotoxicity. In the future, we will explore structural effects on the decorating solubilizing moieties to implement G-quadruplex *vs* ds DNA binding selectivity, retaining the PDT activity.

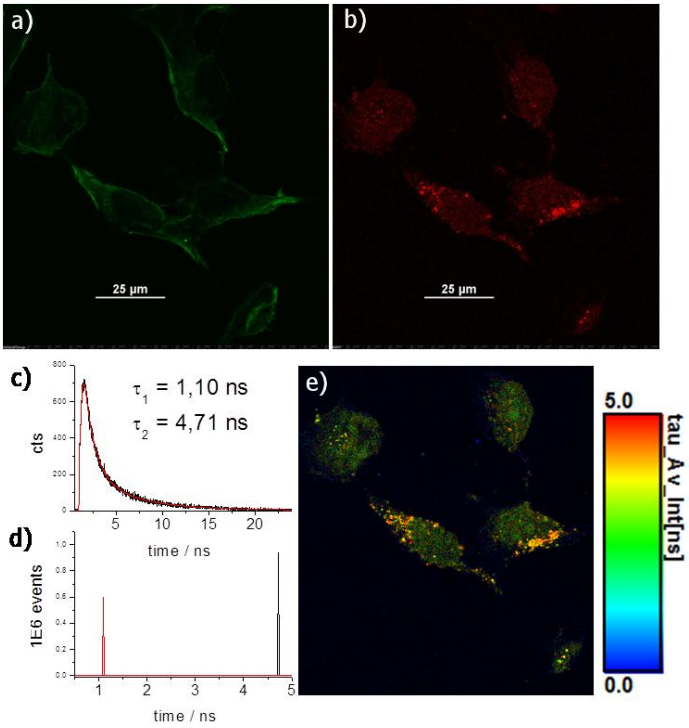

Figure 7. a-b. Confocal fluorescence imaging of fixed BJEHLT fibroblasts: confocal image using a 60X oil immersion objective and exciting at 488 nm (a) and 640 nm (b) recording emission in the 520/40 and 680/70 nm windows, respectively; **c.** fluorescence decay calculated for an ROI in the nucleus and fitted with a biexponential function; **d.** distribution of the lifetime intensity of the image in figure e; **e.** fluorescence lifetime image as a function of the average lifetime with values indicated by the color scale bar.

Experimental

Absorption and fluorescence spectra: UV-visible absorption spectra were recorded on a standard Perkin Elmer λ650 spectrophotometer. Fluorescence spectra were measured using 1 nm steps and 0.5-1 s dwell time. Slits were kept as narrow as possible to 4-8 nm in excitation and 4-8 nm in emission. Where necessary a cut-off filter was used. Right angle detection was used. All the measurements were carried

out at 295 K in quartz cuvettes with path length of 1 cm. All fluorescence spectra have been obtained for air-equilibrated solutions absorbing less than 0.1 at all wavelengths to avoid inner filter effects and re-absorption of emission. Furthermore, they have been corrected for wavelength dependent response of the monochromator/PMT couple.

Fluorescence lifetimes: Fluorescence decays in solution were measured in air-equilibrated solutions for excitation at 637 nm (Hamamatsu pulsed laser with 1 MHz repetition rate) using a time-correlated single photon counting system (TCSPC) (IBH Consultants Ltd., Glasgow, UK) with a resolution of 55 ps per channel. Photons were detected in right angle configuration at 690 nm with a cut-off filter. Fluorescence decay profiles were analyzed with a least-squares method, using multiexponential decay functions (eq. 2) and deconvolution of the instrumental response function. The software package was provided by IBH Consultants Ltd.

The fitting function used is:

$I(t) = b + \Sigma_j a_j e(-t/\tau_j)$ (2)

The fractional intensity and the average fluorescence lifetime are calculated according to the following equations:

$f_i = a_i\tau_i / \Sigma_j a_j\tau_j$ $\tau_{av} = \Sigma_j f_j\tau_j$

Sample Preparation for Titration Studies: For the spectroscopic measurements a 10 mM K^+ phosphate buffer of pH 7.0 was used, with 100 mM KCl/NaCl. Excess of K^+ mimics physiological conditions of cellular compartments where K^+ is abundant. The DNA stock solution was heated at 90 °C for 15 min and then cooled down to room temperature before use. Concentration of the DNA stock solution was determined spectrophotometrically with 0.1 cm cuvets. Compound **1** was dissolved up to a concentration of 7×10^{-5} M in buffer. Aliquots of the dyad and DNA solutions dissolved in the same buffer were mixed together to prepare samples of varying molar ratio. Solutions were kept stirring in the dark for ca. 1 hour before starting the measurements. Water was purified by passage through a Millipore MilliQ system (Millipore SpA, Milan, Italy).

Multiwavelength Global analysis: The best complexation model and the association constants were determined by means of a multivariate global analysis of multiwavelength fluorescence data, analyzing a set of spectra corresponding to different **1**-DNA mixtures. We used the program ReactLab™ Equilibria (Jplus Consulting Pty Ltd). The procedure is based on singular value decomposition (SVD) and non linear regression modelling by the Levenberg-Marquardt method. The analysis also afforded the individual fluorescence spectra of the complexes. The software allows comparison of experimental data and calculated values to evaluate goodness of the fit.

Cell cultures and treatments

Hela human cervical cancer cells, U2OS osteosarcoma cells, MCF7 and MCF7 breast cancer cells resistant to Adriamycin (MCF7-ADR) were purchased from ATCC and maintained in D-MEM supplemented with 10% FCS. BJEHLT cells were obtained and maintained as previously described (Leonetti et al 2004).

NDI **1** and AS1411 powders were dissolved in 100 mM KCl and filtered. Before addition to the cell medium AS1411 was warmed at 90°C, cooled at R.T. to allow the G-quadruplex formation, and then complexed with **1** in a 2:1 molar ratio.

The photodynamic therapy (PDT) experiment was performed as follows: cells were seeded $5x10^4$ cells/well in 6-well plates and treated for 12 hours with 10 μM **1** or left untreated. Then the medium was replaced with PBS containing Mg^{2++} and Ca^{2++} and the cells immediately irradiated with $25J/cm^2$ red light centered at 630 nm (Akilite C128 Lamp, Galderma, UK). Soon after irradiation the cells were re-incubated with complete medium for other 72 hours and cell viability was determined daily. DNA damage induction was determined 24 hours after PDT.

Immunofluorescence: Cultured cells were fixed in 2% formaldehyde and permeabilized in 0.25% Triton X100 in PBS for 5 min at room temperature. For immunolabeling experiments, cells were incubated with the anti-γH2AX mouse mAb (Millipore). Then cells were washed in PBS and incubated with the FITC conjugated Goat anti Mouse (Jackson ImmunoResearch, West Grove, PA, USA) secondary antibody. Nuclei were counterstained with DAPI (Sigma). Fluorescence signals were recorded by using a Leica DMIRE2 microscope equipped with a Leica DFC 350FX camera and elaborated by a Leica FW4000 deconvolution software (Leica, Solms, Germany).

FACS analysis: Hela and BJEHLT cells were seeded $5x10^4$ cells/well in 6-well plates and treated for 6 or 16 hours with 5 μM **1** alone or complexed with the AS1411 G-quadruplex, or left untreated. At each time point, cells were washed three times with PBS, detached from the plates by using Trypsin/EDTA, washed three times and resuspended in PBS.

Flow cytometric measurements and data were performed on a BD Accuri ™ C6 (BD Biosciences, San Jose, CA) equipped with 488- and 640-nm excitation lasers measuring signals from FL4 fluorescence channel (ext. 640 nm, emi. 663/687 nm).

MTT assay: BJEHLT and HeLa cells were seeded at $5x10^3$ cells/well in a 96-well plate in complete medium. After 24 hours cells were treated with NDI and AS1411, alone and in combination, or left untreated (6 replicas/point). Viability of cells was estimated at day 3, 5 and 7 after treatment by adding the MTT solution (Sigma-Aldrich, 5 mg/mL in phosphate-buffered saline; 20 μL/well) to the cell medium, and leaving the plates incubated for another 4 hrs at 37°C to allow the formation of purple formazan crystals. After removing the media, the crystals were dissolved in 200 μL isopropanol per well. OD at 540 nm was determined on microplate reader.

Confocal Fluorescence Imaging: Fluorescence confocal imaging was performed on an inverted Nikon Ti-E microscope (Nikon Co., Shinjuku, Japan). The confocal fluorescence microscope Nikon A1 is equipped with an Argon ion CW laser and 640 nm CW diode laser as well as a 637 nm pulsed/CW diode lasers (PicoQuant GmbH, Berlin, Germany). Images were collected using a Nikon Plan Apo VC 60X oil immersion objective with NA 1.40. Filters were set to register the autofluorescence of cells in the 500-550 nm range and the fluorescence of compound **1** in the 660-740 nm range.

Fluorescence lifetime imaging was performed exciting with the pulsed 637 nm diode laser and collecting photons with

integrated PicoHarp 300 electronics (PicoQuant GmbH, Berlin, Germany) for TCSPC measurements. Histograms of collected photons consist in 1600 channels each with 16 ps width. A single-photon avalanche diode detector equipped with a 695 to 735 nm bandpass filter was used as detector. The repetition rate of the pulsed excitation at 637 nm was 40 MHz. The instrument response function of the system is approximately 220 ps. The fluorescence decay fit was performed on the histogram calculated for a region of interest corresponding to the nucleus in the sample image. The fluorescence decay profile was analyzed with a least-squares method, using biexponential decay function provided by Picoquant SymPhoTime software. Calculated Instrumental Response Function was used for reconvolution

Acknowledgements

We gratefully acknowledge the Italian Association for Cancer Research for financial support. [Grant 14708 to M.F.; 16910 to A.B. and 17121 to E.S.].

Notes and references

1. F. Doria, V. Amendola, V. Grande, G. Bergamaschi and M. Freccero, *Sens. Actuator B-Chem.*, 2015, **212**, 137-144; F. Doria, M. Folini, V. Grande, G. Cimino-Reale, N. Zaffaroni and M. Freccero, *Org. Biomol. Chem.*, 2015, **13**, 570-576.

2. F. Doria, A. Oppi, F. Manoli, S. Botti, N. Kandoth, V. Grande, I. Manet and M. Freccero, *Chem. Commun.*, 2015, **51**, 9105-9108.

3. F. Doria, M. Nadai, G. Sattin, L. Pasotti, S. N. Richter and M. Freccero, *Org. Biomol. Chem.*, 2012, **10**, 3830-3840.

4. M. Nadai, F. Doria, M. Di Antonio, G. Sattin, L. Germani, C. Percivalle, M. Palumbo, S. N. Richter and M. Freccero, *Biochimie*, 2011, **93**, 1328-1340; M. Di Antonio, F. Doria, S. N. Richter, C. Bertipaglia, M. Mella, C. Sissi, M. Palumbo and M. Freccero, *J. Am. Chem. Soc.*, 2009, **131**, 13132-13141.

5. Y. Esaki, M. M. Islam, S. Fujii, S. Sato and S. Takenaka, *Chem. Commun.*, 2014, **50**, 5967-5969; I. Czerwinska, S. Sato, B. Juskowiak and S. Takenaka, *Bioorg. Med. Chem.*, 2014, **22**, 2593-2601.

6. C. Marchetti, A. Minarini, V. Tumiatti, F. Moraca, L. Parrotta, S. Alcaro, R. Rigo, C. Sissi, M. Gunaratnam, S. A. Ohnmacht, S. Neidle and A. Milelli, *Bioorg. Med. Chem.*, 2015, **23**, 3819-3830.

7. M. Micco, G. W. Collie, A. G. Dale, S. A. Ohnmacht, I. Pazitna, M. Gunaratnam, A. P. Reszka and S. Neidle, *J. Med. Chem.*, 2013, **56**, 2959-2974.

8. S. M. Hampel, A. Sidibe, M. Gunaratnam, J.-F. o. Riou and S. Neidle, *Bioorg. Med. Chem. Lett.*, 2010, **20**, 6459-6463; Z. Ou, Y. Qian, Y. Gao, Y. Wang, G. Yang, Y. Li, K. Jiang and X. Wang, *RSC Adv.*, 2016, **6**, 36923-36931.

9. F. Cuenca, O. Greciano, M. Gunaratnam, S. Haider, D. Munnur, R. Nanjunda, W. D. Wilson and S. Neidle, *Bioorg. Med. Chem. Lett.*, 2008, **18**, 1668-1673.

10. C. Röger and F. Würthner, *J. Org. Chem.*, 2007, **72**, 8070-8075; F. Würthner, S. Ahmed, C. Thalacker and T. Debaerdemaeker, *Chem.-Eur. J.*, 2002, **8**, 4742-4750.

11. F. Doria, I. Manet, V. Grande, S. Monti and M. Freccero, *J. Org. Chem.*, 2013, **78**, 8065-8073.

12. J. P. Celli, B. Q. Spring, I. Rizvi, C. L. Evans, K. S. Samkoe, S. Verma, B. W. Pogue and T. Hasan, *Chem. Rev.*, 2010, **110**, 2795-2838.

13. J. Dai, C. Punchihewa, A. Ambrus, D. Chen, R. A. Jones and D. Yang, *Nucl. Acids Res.*, 2007, **35**, 2440-2450; A. Ambrus, D. Chen, J. Dai, T. Bialis, R. A. Jones and D. Yang, *Nucl. Acids Res.*, 2006, **34**, 2723-2735.

14. R. I. Mathad, E. Hatzakis, J. Dai and D. Yang, *Nucl. Acids Res.*, 2011, **39**, 9023-9033.

15. A. T. n. Phan, Y. S. Modi and D. J. Patel, *J. Am. Chem. Soc.*, 2004, **126**, 8710-8716.

16. M. M. Dailey, M. C. Miller, P. J. Bates, A. N. Lane and J. O. Trent, *Nucl. Acids Res.*, 2010, **38**, 4877-4888.

17. G. W. Collie, R. Promontorio, S. M. Hampel, M. Micco, S. Neidle and G. N. Parkinson, *J. Am. Chem. Soc.*, 2012, **134**, 2723-2731.

18. M. Micco, G. W. Collie, A. G. Dale, S. A. Ohnmacht, I. Pazitna, M. Gunaratnam, A. P. Reszka and S. Neidle, *J. Med. Chem.*, 2013, **56**, 2959-2974.

19. F. Doria, M. Nadai, M. Folini, M. Di Antonio, L. Germani, C. Percivalle, C. Sissi, N. Zaffaroni, S. Alcaro, A. Artese, S. N. Richter and M. Freccero, *Org. Biomol. Chem.*, 2012, **10**, 2798-2806.

20. F. Doria, M. Nadai, M. Folini, M. Scalabrin, L. Germani, G. Sattin, M. Mella, M. Palumbo, N. Zaffaroni, D. Fabris, M. Freccero and S. N. Richter, *Chem.-Eur. J.*, 2013, **19**, 78-81.

21. A. Siddiqui-Jain, C. L. Grand, D. J. Bearss and L. H. Hurley, *Proc Natl Acad Sci U S A*, 2002, **99**, 11593-11598; S. Balasubramanian, L. H. Hurley and S. Neidle, *Nat. Rev. Drug Discov.*, 2011, **10**, 261-275; J. L. Huppert and S. Balasubramanian, *Nucl. Acids Res.*, 2005, **33**, 2908-2916; J. L. Huppert and S. Balasubramanian, *Nucl. Acids Res.*, 2007, **35**, 406-413.

22. B. Pagano, J. Amato, N. Iaccarino, C. Cingolani, P. Zizza, A. Biroccio, E. Novellino and A. Randazzo, *Chemmedchem*, 2015, **10**, 640-649; S. Ray, J. N. Bandaria, M. H. Qureshi, A. Yildiz and H. Balci, *Proc Natl Acad Sci U S A*, 2014, **111**, 2990-2995.

23. A. Shivalingam, M. A. Izquierdo, A. L. Marois, A. Vysniauskas, K. Suhling, M. K. Kuimova and R. Vilar, *Nat. Commun.*, 2015, **6**; G. F. Salgado, C. Cazenave, A. Kerkour and J.-L. Mergny, *Chem. Sci.*, 2015, **6**, 3314-3320; G. Biffi, D. Tannahill, J. McCafferty and S. Balasubramanian, *Nat. Chem.*, 2013, **5**, 182-186.

24. A. A. Neumann and R. R. Reddel, *Nat. Rev. Cancer*, 2002, **2**, 879-884.

25. S. A. Ohnmacht, C. Marchetti, M. Gunaratnam, R. J. Besser, S. M. Haider, G. Di Vita, H. L. Lowe, M. Mellinas-Gomez, S. Diocou, M. Robson, J. Sponer, B. Islam, R. B. Pedley, J. A. Hartley and S. Neidle, *Sci. Rep.*, 2015, **5**, 11.

26. P. J. Bates, S. Jueliger, A. C. Girvan, Y. Teng, L. Casson, S. Thomas, Y. C. Mi, X. H. Xu, S. Barve, D. M. Miller and J. O. Trent, *Clin. Cancer Res.*, 2005, **11**, 9114S-9115S.

27. F. Mongelard and P. Bouvet, *Curr. Opin. Mol. Ther.*, 2010, **12**, 107-114; R. K. Stuart, K. Stockerl-Goldstein, M. Cooper, M. Devetten, R. Herzig, B. Medeiros, G. Schiller, A. Wei, G. Acton and D. Rizzieri, *J. Clin. Oncol.*, 2009, **27**, 2.

28. J. M. Zhang, R. E. Chen, F. Q. Chen, M. W. Chen and Y. T. Wang, *J. Control. Release*, 2015, **213**, E137-E138; X. Li, Q. Zhao and L. Qiu, *J. Control. Release*, 2013, **171**, 152-162.
29. J. Zhou and J. J. Rossi, *Mol Ther Nucleic Acids*, 2014, **3**, e169.
30. Y. A. Shieh, S. J. Yang, M. F. Wei and M. J. Shieh, *ACS Nano*, 2010, **4**, 1433-1442.
31. Z. Huang, *Technology in cancer research & treatment*, 2005, **4**, 283-293.
32. J. E. Rogers, S. J. Weiss and L. A. Kelly, *J. Amer. Chem. Soc.*, 2000, **122**, 427-436.
33. P. Changenet-Barret, T. Gustavsson, D. Markovitsi and I. Manet, *ChemPhysChem*, 2016, **17**, 1264.
34. We also measured the fluorescence decays of the heated mixtures and performed a similar analysis with 4-exponential fitting function fixing the 4.84 ns lifetime. The three lifetimes calculated were 0.26, 1.91 and 6.75 ns and are very similar to the analysis above. The pre-exponential factors however slightly differ. The concentration of the species with lifetime 0.26 ns was in line with the concentration of the 1:2 complex while 1.91 and 6.75 belong to species with concentrations corresponding to that of the 1:1 complex.
35. Z. F. Wang and T. C. Chang, *Nucl. Acids Res.*, 2012, **40**, 8711-8720; V. Viglasky, L. Bauer, K. Tluckova and P. Javorsky, *J. Nucl. Acids*, 2010, **2010**.
36. X. Ming, W. Ju, H. Wu, R. R. Tidwell, J. E. Hall and D. R. Thakker, *Drug Metab Dispos*, 2009, **37**, 424-430.
37. T. J. Jensen, M. G. a. H. Vicente, R. Luguya, J. Norton, F. R. Fronczek and K. M. Smith, *J. Photochem. Photobiol. B*, 2010, **100**, 100-111; F. Ricchelli, L. Franchi, G. Miotto, L. Borsetto, S. Gobbo, P. Nikolov, J. C. Bommer and E. Reddi, *Int. J. Biochem. & Cell Biol.,* 2005, **37**, 306-319.
38. S. M. Hampel, A. Pepe, K. M. Greulich-Bode, S. V. Malhotra, A. P. Reszka, S. Veith, P. Boukamp and S. Neidle, *Mol. Pharmacol.*, 2013, **83**, 470-480.
39. C. R. Fairchild, J. A. Moscow, E. E. O'Brien and K. H. Cowan, *Mol. Pharmacol.*, 1990, **37**, 801-809.

Journal Name

ARTICLE

Graphical content

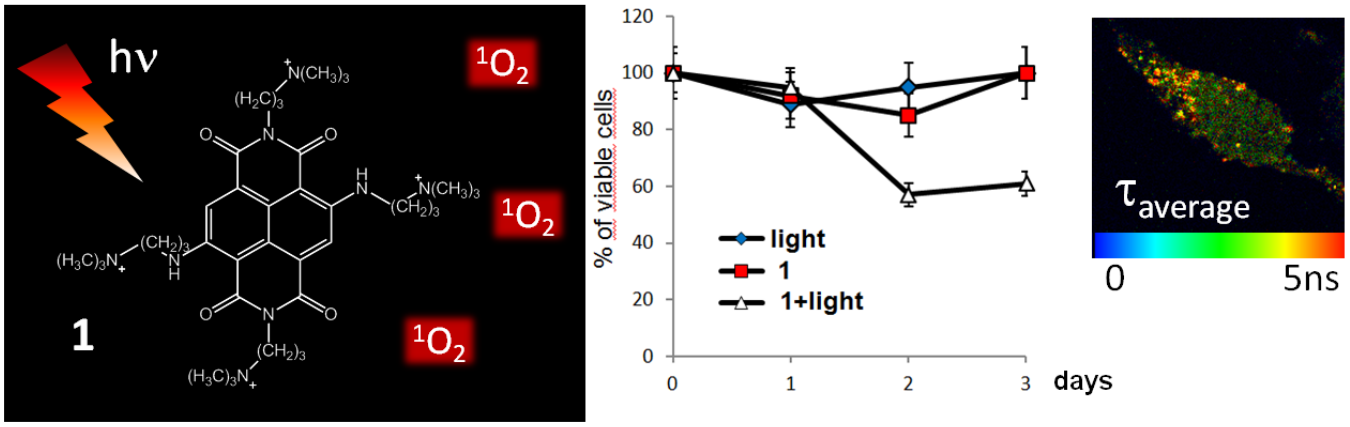

We describe the bimodal activity of a water-soluble tetracationic Naphthalene Diimide as red light emitter for fluorescence imaging, including fluorescence-lifetime imaging, and singlet oxygen photosensitizer, inducing photocytotoxicity in cancer cells.